

Robust Convex Model Predictive Control with collision avoidance guarantees for robot manipulators

Bernhard Wullt¹, Johannes Köhler², Per Mattsson³, Mikeal Norrlöf¹, Thomas B. Schön³

Abstract—Industrial manipulators are normally operated in cluttered environments, making safe motion planning important. Furthermore, the presence of model-uncertainties make safe motion planning more difficult. Therefore, in practice the speed is limited in order to reduce the effect of disturbances. There is a need for control methods that can guarantee safe motions that can be executed fast. We address this need by suggesting a novel model predictive control (MPC) solution for manipulators, where our two main components are a robust tube MPC and a corridor planning algorithm to obtain collision-free motion. Our solution results in a convex MPC, which we can solve fast, making our method practically useful. We demonstrate the efficacy of our method in a simulated environment with a 6 DOF industrial robot operating in cluttered environments with uncertainties in model parameters. We outperform benchmark methods, both in terms of being able to work under higher levels of model uncertainties, while also yielding faster motion.

I. INTRODUCTION

Motion planning for robot manipulators is an important problem for industrial applications due to the natural presence of surrounding obstacles. This problem has been extensively studied and it is typically addressed with an efficient pipeline that decouples the problem into smaller sub-problems [1]. First, a collision-free path is found using a sampling-based planner [2], [3], which is possibly also post-processed [4]. Next, the path is time scaled using the model of our system, e.g., by solving a convex optimization problem [5], which results in a dynamically feasible trajectory. Finally, feedback-linearization is used [6], [7] with the full dynamics model to track the trajectory closely.

Although the approach is efficient and successfully solves the problem, accurate modeling becomes paramount. Furthermore, since the path planning approach relies on collision-detection, we are forced to stay exactly on the path, since that is only where it has been certified to be collision-free. This becomes more challenging through uncertainties in the model parameters, which propagates through the coupled dynamics, resulting in state and input dependent model-mismatch. The current pipeline addresses this issue by moving sufficiently slow, such that the effect of model mismatch can be effectively attenuated. A key limiting factor is the lack of methods to effectively ensure robustness also for faster motions.

We address the missing robustness guarantees, allowing

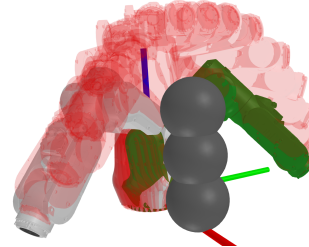


Fig. 1: Illustration of our convex robust MPC. We produce collision-free motion that is robust to model-errors. The closed loop trajectory (transparent red meshes) connect a given start and goal state (white and green meshes) while avoiding the obstacles (gray spheres).

us to enable safe and fast motion planning in cluttered environments. We realize this through two main contributions:

- We use feedback-linearization to obtain a linear prediction model and derive a state and input dependent upper bound on the resulting model error. We design a tube based model predictive controller (MPC) that utilizes this bound and optimizes the tube size to reduce conservatism.
- To propagate the tube in the configuration space, we employ a signed configuration distance function (SCDF), which outputs collision-free balls in the configuration space. This allows us to formulate simple convex constraints for obstacle avoidance, while also allowing us to propagate the tube in a collision-free region, enabling quick collision-free progress towards the goal.

The result is a convex MPC problem, which we can solve efficiently, and a simple approach to guide it to its goal state, resulting in fast and safe motion. We show the validity of our approach through simulations of an industrial 6 DOF (see Figure 1) robot in cluttered environments. This is the first construction of a convex MPC that guarantees collision avoidance for nonlinear uncertain dynamics of 6 DOF industrial robots. Our solution is open-sourced:

https://github.com/whiterabbitfollow/rob_cvx_mpc_rob_man.

Outline: Section II presents related work. We introduce the notation in Section III and the problem formulation in Section IV. Next, we derive our novel robust motion planning solution for manipulators in Section V. Obstacle avoidance is included in Section VI by proposing the concept of corridor planning and deriving simple convex constraints ensuring collision-free motion. We verify our approach in numerical experiments (Section VII) and end with conclusions (Section VIII).

¹ ABB Robotics, Sweden.

² Institute for Dynamic Systems and Control, ETH Zurich, Switzerland.

³ Department of Information Technology, Uppsala University, Sweden.

This research was supported by the Wallenberg AI, Autonomous Systems and Software Program (WASP) funded by Knut and Alice Wallenberg Foundation.

II. RELATED WORK

Over the past decade, a lot of methods have been developed in order to produce convex collision-free regions in the configuration space, which shed new light on how to conduct motion planning for manipulators. In [8], [9] an optimization problem is solved iteratively to enlarge an ellipsoid, while [10], [11] instead use learning to produce collision-free regions in the form of balls. These tools enable new approaches for motion planning, instead of staying on a path, one can be inside a corridor, i.e. a collision-free region. The concept of corridors [12] is well known for drones [13], [14], but for manipulators the non-trivial mapping of world space obstacles to the configuration space presents a challenge. In [15], the corridor concept is used to address robustness through funnel control. However, funnel control often loses its guarantees in the presence of actuator constraints and is in general susceptible to amplifying noise.

Our approach instead relies on MPC [16], which guarantees satisfaction of state and input constraints. The main idea behind MPC is to predict a future trajectory of a dynamical system and optimize the trajectory w.r.t. a user-defined loss, e.g. minimize path length. Applications of MPC to robot manipulators are, for example, presented in [17], [18], [19]. However, these approaches are computationally expensive, can only cover simple collision avoidance constraints or none at all, or are conservative. In particular, [17], [18] formulate non-linear MPC schemes, which becomes computationally expensive. Only simplified collision avoidance constraints are treated in [17], while [18], [19] do not address obstacle avoidance at all. The robustness guarantees in [17], [19] are based on a constant (worst-case) bound on the model-mismatch, which neglects the state/input dependent nature of modeling errors, resulting in significant conservatism, while [18] lacks robustness guarantees. Compared to mentioned work, we guarantee obstacle avoidance through a SCDF, which gives us convex obstacle avoidance constraints. Furthermore, we address robustness and propose a less conservative approach, where we derive a state and input dependent model error. Finally, our resulting MPC is convex, which we can solve fast.

Due to the inherent computational complexity of solving non-linear MPC problems, many researchers focus on learning explicit policies [17], [20], [21] which reduces the computational cost. This approach can be successful, but struggles to generalize to complex obstacle scenarios with a large number of possible input permutations in the obstacle setup. Instead of directly learning a policy, the proposed approach learns convex collision-free regions. We rely on [11], which is a deep-learning based approach to approximate a SCDF, i.e. a signed distance function (SDF) expressed in the configuration space. This allows us to focus on learning a single SCDF for the desired robotic arm and class of obstacles, e.g. spheres or boxes. Multiple obstacles can then be combined simply by querying for the individual distances and combining them through a min-operator. This results

in a tractable learning problem, which breaks the potential explosion in obstacle input permutation. Furthermore, the learned SCDF allows for changes or introduction of new obstacles, since the positions and shapes are included as inputs to the network. Thus, no learning has to be re-done if the environment changes, making our approach flexible and practically useful.

III. NOTATION

The set of positive real numbers is denoted by \mathbb{R}_+ . We denote the set of integers a to b , i.e. $\{a, a+1, \dots, b\}$ by $\mathbb{N}_{a:b}$. The set of n dimensional positive definite matrices is denoted by \mathbb{S}_{++}^n . For a vector $\mathbf{x} \in \mathbb{R}^n$, we denote the 2-norm and infinity-norm as $\|\mathbf{x}\| = \sqrt{\mathbf{x}^\top \mathbf{x}}$ and $\|\mathbf{x}\|_\infty = \max_i |\mathbf{x}_i|$. For a matrix $\mathbf{A} \in \mathbb{R}^{n \times m}$, $\|\mathbf{A}\|$ is the induced matrix norm, i.e., the largest singular value of \mathbf{A} . The weighted vector norm, denoted by $\|\mathbf{x}\|_{\mathbf{A}}$, is defined as $\sqrt{\mathbf{x}^\top \mathbf{A} \mathbf{x}}$. We denote the symmetric matrix square root of a positive semi-definite matrix \mathbf{A} as $\mathbf{A}^{1/2}$. The vectors $\mathbf{1}_n$ and $\mathbf{0}_n$ denotes an n dimensional vector of ones and zeros, respectively. The identity matrix is denoted as \mathbf{I} . We express the operation of stacking two column vectors as $(\mathbf{a}, \mathbf{b}) = [\mathbf{a}^\top, \mathbf{b}^\top]^\top$. Finally, the function $\text{diag}(\cdot) : \mathbb{R}^n \mapsto \mathbb{R}^{n \times n}$, maps an n dimensional vector into a diagonal matrix.

IV. PROBLEM FORMULATION

Consider a robot operating in the world space, $\mathcal{W} \subset \mathbb{R}^3$. The exact description of the robot body is given by its configuration $\mathbf{q} \in \mathcal{C}$, where $\mathcal{C} \subset \mathbb{R}^{n_c}$ is the configuration space. The robot dynamics has the following form

$$\mathbf{u} = \mathbf{M}(\mathbf{q})\ddot{\mathbf{q}} + \mathbf{C}(\mathbf{q}, \dot{\mathbf{q}})\dot{\mathbf{q}} + \mathbf{g}(\mathbf{q}). \quad (1)$$

In the above, $\dot{\mathbf{q}} \in \mathcal{V}$, $\mathbf{u} \in \mathcal{U}$, denote the velocity and control input, constrained to lie in their corresponding sets $\mathcal{V} \subset \mathbb{R}^{n_c}$ and $\mathcal{U} \subset \mathbb{R}^{n_c}$. Furthermore, $\mathbf{M} : \mathbb{R}^{n_c} \mapsto \mathbb{R}^{n_c \times n_c}$, $\mathbf{C} : \mathbb{R}^{n_c} \times \mathbb{R}^{n_c} \mapsto \mathbb{R}^{n_c \times n_c}$, $\mathbf{g} : \mathbb{R}^{n_c} \mapsto \mathbb{R}^{n_c}$, denote the mass matrix, coupling matrix (Coriolis and damping), and gravity vector functions, respectively. We assume incomplete knowledge of the model parameters of (1), separating the model into nominal (known) and uncertain terms:

$$\begin{aligned} \mathbf{M}(\mathbf{q}) &= \mathbf{M}_0(\mathbf{q}) + \mathbf{M}_\theta(\mathbf{q}), \\ \mathbf{C}(\mathbf{q}, \dot{\mathbf{q}}) &= \mathbf{C}_0(\mathbf{q}, \dot{\mathbf{q}}) + \mathbf{C}_\theta(\mathbf{q}, \dot{\mathbf{q}}), \\ \mathbf{g}(\mathbf{q}) &= \mathbf{g}_0(\mathbf{q}) + \mathbf{g}_\theta(\mathbf{q}), \end{aligned}$$

where a null index denotes nominal terms, and error terms are indexed by a parameter vector $\theta \in \Theta$, where $\Theta \subset \mathbb{R}^{n_p}$ is a known parameter set and θ is the unknown model parameter. We assume that the sets \mathcal{C} , \mathcal{V} and \mathcal{U} are hyperboxes, and that measurements of \mathbf{q} and $\dot{\mathbf{q}}$ are readily available.

The robot is surrounded by n_o obstacles $\mathcal{O} = \bigcup_{i=1}^{n_o} \mathcal{O}_i$, where $\mathcal{O}_i \subset \mathcal{W}$. The set of points covered by the robot body in configuration \mathbf{q} is expressed as $\mathcal{FK}(\mathbf{q}) \subset \mathcal{W}$. We define the free space as $\mathcal{C}_f = \{\mathbf{q} \in \mathcal{C} \mid \mathcal{FK}(\mathbf{q}) \cap \mathcal{O} = \emptyset\}$ and the obstacle region as $\mathcal{C}_o = \mathcal{C} \setminus \mathcal{C}_f$.

Overall, our goal is to design a controller that steers the robot from a given start configuration \mathbf{q}_s to a goal configuration \mathbf{q}_g , while ensuring that the resulting trajectory satisfies constraints on velocity, torque, and is collision-free, i.e. $\mathbf{q}(t) \in \mathcal{C}_f$, $\dot{\mathbf{q}}(t) \in \mathcal{V}$, $\mathbf{u}(t) \in \mathcal{U}$, $\forall t \geq 0$, for any considered model parameters $\theta \in \Theta$.

V. ROBUST CONVEX MPC FOR MANIPULATORS

In this section, we focus on obtaining a motion planning solution that comes with robustness guarantees, for the moment ignoring obstacle avoidance, which we address in the subsequent section.

A key feature we aim for in our design is that the resulting MPC problem can be solved fast. Hence, we want a convex solution, which therefore requires convex constraints and linear prediction models. First, we utilize feedback-linearization to obtain a linear model and a suitable bound on the un-cancelled non-linearities (Section V-A). To ensure robustness, we predict a scaled tube around a nominal prediction such that it contains the true (unknown) system response. We use an auxiliary controller and an ellipsoid tube to derive an expression for the tube dynamics (Section V-B). Since the feedback-linearization yields non-convex input constraints, we present a sampling-based approach to produce a convex input constraint that ensures satisfaction of the torque constraints (Section V-C). Finally, we present our suggested convex robust MPC in Section V-D, including the theoretical analysis.

A. Feedback linearization and model error

In order to obtain a convex optimization problem, we have to obtain a linear prediction model. We use feedback linearization (FL [6]) to realize this, i.e., we cancel the (known) non-linear terms in the dynamics using a feedback:

$$\mathbf{u} = \pi_{\text{FL}}(\mathbf{q}, \dot{\mathbf{q}}, \mathbf{a}) = \mathbf{M}_0(\mathbf{q})\mathbf{a} + \mathbf{C}_0(\mathbf{q}, \dot{\mathbf{q}})\dot{\mathbf{q}} + \mathbf{g}_0(\mathbf{q}), \quad (2)$$

where $\mathbf{a} \in \mathbb{R}^{n_c}$ is the desired acceleration. Using the above feedback in the dynamics (1) yields

$$\ddot{\mathbf{q}} = \mathbf{a} + \Delta_\theta(\mathbf{q}, \dot{\mathbf{q}}, \mathbf{a}), \quad (3)$$

$$\Delta_\theta(\mathbf{q}, \dot{\mathbf{q}}, \mathbf{a}) = \tilde{\mathbf{M}}_\theta(\mathbf{q})\mathbf{a} + \tilde{\mathbf{C}}_\theta(\mathbf{q}, \dot{\mathbf{q}})\dot{\mathbf{q}} + \tilde{\mathbf{g}}_\theta(\mathbf{q}), \quad (4)$$

where $\tilde{\mathbf{M}}_\theta : \mathbb{R}^{n_c} \mapsto \mathbb{R}^{n_c \times n_c}$, $\tilde{\mathbf{C}}_\theta : \mathbb{R}^{n_c} \mapsto \mathbb{R}^{n_c \times n_c}$ and $\tilde{\mathbf{g}}_\theta : \mathbb{R}^{n_c} \mapsto \mathbb{R}^{n_c}$ are errors parameterized by the uncertain model parameter $\theta \in \Theta$, see Appendix A for the derivation. We note that this transformation does not introduce any approximations, but simply shows that the uncertain robot dynamics with the feedback behaves equivalent to a double integrator subject to an additional nonlinear function Δ_θ , that depends on the uncertain model parameters θ . Transforming the system to discrete time using Euler discretization results in

$$\mathbf{x}(k+1) = \mathbf{A}\mathbf{x}(k) + \mathbf{B}(\mathbf{a}(k)) + \Delta_\theta(\mathbf{q}(k), \dot{\mathbf{q}}(k), \mathbf{a}(k)), \quad (5)$$

where, $k \in \mathbb{N}$ is the discrete time index, $\mathbf{x} = (\mathbf{q}, \dot{\mathbf{q}}) \in \mathcal{X} := \mathcal{C} \times \mathcal{V} \subset \mathbb{R}^{n_x}$ is the state with $n_x = 2 \cdot n_c$, $\mathbf{A} \in \mathbb{R}^{n_x \times n_x}$

and $\mathbf{B} \in \mathbb{R}^{n_x \times n_c}$ denote the dynamics and control matrices, respectively. We obtain a bound on the norm of the model error from the following proposition.

Proposition 1. *For all $\mathbf{x} = (\mathbf{q}, \dot{\mathbf{q}}) \in \mathcal{X}$, $\mathbf{a} \in \mathcal{A}$ and $\theta \in \Theta$, we have*

$$\|\Delta_\theta(\mathbf{q}, \dot{\mathbf{q}}, \mathbf{a})\| \leq \beta(\mathbf{x}, \mathbf{a}) := a \|\mathbf{a}\| + b \|\dot{\mathbf{q}}\| + c. \quad (6)$$

with a, b, c according to (7)–(9).

Proof. Using the triangle inequality and the property $\|\mathbf{Ax}\| \leq \|\mathbf{A}\| \|\mathbf{x}\|$ [22] on the individual terms of expression (4), we end up with the bound in (6), where $a, b, c \in \mathbb{R}_+$ are computed as

$$a = \max_{\theta \in \Theta, \mathbf{q} \in \mathcal{C}} \|\tilde{\mathbf{M}}_\theta(\mathbf{q})\|, \quad (7)$$

$$b = \max_{\theta \in \Theta, (\mathbf{q}, \dot{\mathbf{q}}) \in \mathcal{X}} \|\tilde{\mathbf{C}}_\theta(\mathbf{q}, \dot{\mathbf{q}})\|, \quad (8)$$

$$c = \max_{\theta \in \Theta, \mathbf{q} \in \mathcal{C}} \|\tilde{\mathbf{g}}_\theta(\mathbf{q})\|. \quad (9)$$

The closed-form expressions of the functions introduced above are presented in Appendix A. \square

This bound highlights that the error depends significantly on the velocity and acceleration, crucial knowledge that the controller will leverage for safe and efficient planning. We note that the constants a, b and c can be well approximated by sampling.

B. Auxiliary controller and tube dynamics

To attenuate the effects of the model errors over a prediction horizon, we use an auxiliary controller, with the following control law

$$\mathbf{a} = \bar{\mathbf{a}} + \mathbf{K}(\mathbf{x} - \bar{\mathbf{x}}). \quad (10)$$

The matrix $\mathbf{K} \in \mathbb{R}^{n_u \times n_x}$, is termed as the gain matrix, $\bar{\mathbf{a}} \in \mathbb{R}^{n_u}$ and $\bar{\mathbf{x}} \in \mathbb{R}^{n_x}$ are the reference control and states, respectively. We compute the gain matrix that satisfies the following requirement

$$\|(\mathbf{A} + \mathbf{BK})\mathbf{x}\|_P \leq \rho \|\mathbf{x}\|_P, \quad \forall \mathbf{x} \in \mathbb{R}^{n_x}, \quad (11)$$

where $\rho \in (0, 1)$ is a contraction rate and $\mathbf{P} \in \mathbb{S}_{++}^{n_x}$ is referred to as the Lyapunov matrix. We obtain \mathbf{P} and \mathbf{K} satisfying (11) by solving a convex optimization problem offline, see Appendix B for details. The Lyapunov matrix \mathbf{P} allows us to trace out an ellipsoid in state and input space

$$\mathcal{E}(\delta) = \{\mathbf{x} \in \mathbb{R}^{n_x} \mid \|\mathbf{x}\|_P \leq \delta\}, \quad (12a)$$

$$\mathcal{E}_\mathbf{a}(\delta) = \{\mathbf{a} = \mathbf{K}\mathbf{x} \in \mathbb{R}^{n_u} \mid \mathbf{x} \in \mathcal{E}(\delta)\}, \quad (12b)$$

where the size of the ellipsoid is controlled by the scaling $\delta \in \mathbb{R}_+$. The following proposition shows how we can adjust the scaling such that the uncertain system (5) remains inside the ellipsoid (12) around the nominal prediction.

Proposition 2. *For any $\|\mathbf{x} - \bar{\mathbf{x}}\|_P \leq \delta$, $\theta \in \Theta$, we have that $\|\mathbf{x}_+ - \bar{\mathbf{x}}_+\|_P \leq \delta_+$ with $\mathbf{x}_+ \in \mathcal{E}(\delta)$ according to (5), $\bar{\mathbf{x}}_+ = \mathbf{A}\bar{\mathbf{x}} + \mathbf{B}\bar{\mathbf{a}}$, $\mathbf{a} = \bar{\mathbf{a}} + \mathbf{K}(\mathbf{x} - \bar{\mathbf{x}})$ and*

$$\delta_+ = (\rho + dL_\beta)\delta + d\beta(\bar{\mathbf{x}}, \bar{\mathbf{a}}), \quad (13)$$

$$d = \|\mathbf{P}^{1/2}\mathbf{B}\|, \quad (14)$$

$$L_\beta = a \|\mathbf{K}\mathbf{P}^{-1/2}\| + b \|\mathbf{V}\mathbf{P}^{-1/2}\|, \quad (15)$$

with $\mathbf{V} = [\mathbf{0}_{n_c \times n_c}, \mathbf{I}_{n_c \times n_c}]$.

The proof can be found in Appendix C. In the following, we abbreviate $\tilde{\rho} := \rho + dL_\beta$ and we assume that $\tilde{\rho} < 1$. Given $\rho < 1$, this holds if the uncertainty $\|\Delta_\theta\|$ is sufficiently small. Finally, for a steady state with zero velocity/acceleration, the tube size δ converges to a steady state tube size

$$\delta_f := d \cdot c / (1 - \tilde{\rho}) \quad (16)$$

C. Convex feasible acceleration constraints

The process of feedback-linearization results in non-convex input constraint due to the non-linear map in (2). We seek a convex constraint set $\mathbf{a} \in \mathcal{A}$, which ensures that the resulting torque (2) satisfies $\mathbf{u} \in \mathcal{U}$, i.e.:

$$\{\pi_{\text{FL}}(\mathbf{q}, \dot{\mathbf{q}}, \mathbf{a}) \mid (\mathbf{q}, \dot{\mathbf{q}}) \in \mathcal{X}, \mathbf{a} \in \mathcal{A}\} \subseteq \mathcal{U}. \quad (17)$$

We approach this problem using sampling. We start with a box constraint set for the acceleration, $\mathcal{A} \subset \mathbb{R}^{n_c}$, represented in vertex form. Then, we uniformly sample states $(\mathbf{q}, \dot{\mathbf{q}}) \in \mathcal{X}$, for each sampled state and vertex a , we verify condition (17). If the condition is violated at some point, we shrink the acceleration set uniformly by a small amount and then repeat the process until it is satisfied for all states and vertices. When the process is done, we obtain a convex acceleration input-set \mathcal{A} that ensures satisfaction of the torque constraint $\mathbf{u} \in \mathcal{U}$.

D. Robust convex MPC problem

With a convex expression for the model error propagation and convex input constraints established, we can now formulate our robust model predictive control problem as follows:

$$\min_{\bar{\mathbf{X}}, \bar{\mathbf{A}}, \delta} \sum_{i=0}^{H-1} \left[\|\bar{\mathbf{x}}_i - \bar{\mathbf{x}}_H\|_{\mathbf{Q}}^2 + \|\bar{\mathbf{a}}_i\|_{\mathbf{R}}^2 + \delta_i \right] \quad (18a)$$

$$+ \|\bar{\mathbf{x}}_H - \mathbf{x}_g\|_{\mathbf{Q}_e}^2 + \frac{1}{1 - \tilde{\rho}} \delta_H$$

$$\text{s.t. } \|\bar{\mathbf{x}}_0 - \mathbf{x}(k)\|_{\mathbf{P}} \leq \delta_0, \quad (18b)$$

$$\bar{\mathbf{x}}_{i+1} = \bar{\mathbf{A}}\bar{\mathbf{x}}_i + \bar{\mathbf{B}}\bar{\mathbf{a}}_i, \quad (18c)$$

$$\dot{\mathbf{q}}(\bar{\mathbf{x}}_H) = \mathbf{0}_{n_c}, \quad \delta_H \geq \delta_f, \quad \bar{\mathbf{x}}_H \in \mathcal{X} \ominus \mathcal{E}(\delta_H + \epsilon) \quad (18d)$$

$$\delta_{i+1} \geq \tilde{\rho}\delta_i + d\beta(\bar{\mathbf{x}}_i, \bar{\mathbf{a}}_i), \quad (18e)$$

$$\bar{\mathbf{x}}_i \in \mathcal{X} \ominus \mathcal{E}(\delta_i), \quad (18f)$$

$$\bar{\mathbf{a}}_i \in \mathcal{A} \ominus \mathcal{E}_{\mathbf{a}}(\delta_i), \quad i \in \mathbb{N}_{0:H-1}, \quad (18g)$$

using the current state $\mathbf{x}(k)$, the goal state \mathbf{x}_g , user chosen positive definite weight matrices $\mathbf{Q}, \mathbf{Q}_e, \mathbf{R} \in \mathbb{S}_{++}$, $\epsilon > 0$, and a horizon $H \geq 2$. The decision variables are the nominal trajectory, $\bar{\mathbf{X}} = [\bar{\mathbf{x}}_0, \dots, \bar{\mathbf{x}}_H] \in \mathbb{R}^{n_x \times (H+1)}$, the nominal control inputs $\bar{\mathbf{A}} = [\bar{\mathbf{a}}_0, \dots, \bar{\mathbf{a}}_{H-1}] \in \mathbb{R}^{n_u \times H}$ and the tube size $\delta = [\delta_0, \dots, \delta_H]^\top \in \mathbb{R}^H$. In closed-loop operation, we solve (18) with the current measured state $\mathbf{x}(k)$, and then apply $\mathbf{a}(k) = \bar{\mathbf{a}}_0^*$, the first optimized input, to the system. Note that Problem (18) is a convex second-order cone problem, which can be efficiently solved.

The objective, (18a), consists of three parts. The first

part drives the predicted trajectory to the steady-state $\bar{\mathbf{x}}_H$, which acts as an artificial reference (cf. [23]), while keeping the controls small. A second term pushes this artificial reference to the desired goal \mathbf{x}_g . Lastly, we also minimize the tube size δ , with an increased penalty for the last step.

The nominal trajectory starts with a tube around the measured state $\mathbf{x}(k)$ (18b) and evolves according to the linear dynamics (18c). The final state is a steady-state with zero velocity (18d). The scaling of the tube (18e) is according to Proposition 2. Finally, the state and control limits are tightened by the tube size in (18f) and (18g), respectively. The operator \ominus denotes the Pontryagin differences, see Appendix B2 for implementation details. The following theorem summarizes the closed-loop properties.

Theorem 1. Consider the nonlinear system (5) with $\theta \in \Theta$. Suppose that Problem (18) is feasible at $k = 0$. Then, the closed-loop system satisfies:

- *Recursive feasibility:* Problem (18) is feasible $\forall k \in \mathbb{N}$;
- *Constraint satisfaction:* $\mathbf{x}(k) \in \mathcal{X}, \mathbf{a}(k) \in \mathcal{A}, \forall k \in \mathbb{N}$;
- *Convergence:* $\lim_{k \rightarrow \infty} \|\mathbf{x}(k) - \mathbf{x}_g\| = 0$, if $\mathbf{x}_g \in \mathcal{X} \ominus \mathcal{E}(\epsilon + \delta_f)$.

Proof. The proof merges concepts from robust MPC using homothetic tube [24] and MPC for tracking formulations [23], [25].

Part I: Given the optimal solution to problem (18) at time k , we consider the following feasible candidate solution $\bar{\mathbf{X}} = [\bar{\mathbf{x}}_1^*, \dots, \bar{\mathbf{x}}_H^*, \bar{\mathbf{x}}_H^*]$, $\bar{\mathbf{A}} = [\bar{\mathbf{a}}_1^*, \dots, \bar{\mathbf{a}}_{H-1}^*, \mathbf{0}_{n_u}]$, $\delta = [\delta_1^*, \dots, \delta_H^*, \delta_H]$. Here, $\delta_H = \delta_H^*(1 - \tilde{\rho}) + d \cdot c$ according to (18e) with $\beta(\bar{\mathbf{x}}_H, 0) = c$, given that $\bar{\mathbf{x}}_H^*$ is a steady-state using (18d). Furthermore, $\tilde{\rho} < 1$ and $\delta_H^* \geq \delta_f$ (16) ensure that $\delta_H \leq \delta_H^*$ and thus this appended solution also satisfies the tightened constraints (18e) at $i = H$. Lastly, Proposition 2 ensures that this candidate solution also satisfies the initial state constraint (18b) with the new measured state $\mathbf{x}(k+1)$ for any $\theta \in \Theta$.

Part II: Closed-loop constraint satisfaction follows from feasibility of Problem (18), the tightened constraints (18f), (18g), and the fact that $\mathbf{x}(k) - \bar{\mathbf{x}}_0^* \in \mathcal{E}(\delta_0^*), \mathcal{E}(\delta_0^*), \mathbf{a}(k) - \bar{\mathbf{a}}_0^* \in \mathcal{E}_{\mathbf{a}}(\delta_0^*)$ using the definition of the ellipsoids (12) and the initial state constraint (18b).

Part III: Let us denote the optimal cost of Problem (18) at time k by $\mathcal{J}(k)^*$. The feasible candidate solution implies

$$\begin{aligned} & \mathcal{J}^*(k+1) - \mathcal{J}^*(k) \\ & \leq -\|\bar{\mathbf{x}}_0^* - \bar{\mathbf{x}}_H^*\|_{\mathbf{Q}}^2 - \|\bar{\mathbf{a}}_0^*\|_{\mathbf{R}}^2 - \delta_0^* + \underbrace{\frac{1}{1 - \tilde{\rho}}(\delta_H - \delta_H^*) + \delta_{H-1}}_{=0} \end{aligned}$$

where the last term cancels given $\delta_H = \tilde{\rho}\delta_{H-1} = \tilde{\rho}\delta_H^*$. Given \mathcal{J}^* non-negative and \mathcal{J}_0^* finite, using this condition in a telescopic sum ensures that, as $k \rightarrow \infty$, $\mathbf{x}(k) = \bar{\mathbf{x}}_0^*$ converges to a steady-state. Lastly, to ensure that this steady-state corresponds to \mathbf{x}_g , we use [25, Lemma 1], which ensures the existence of a uniform constant $d > 0$, such that

$$\|\bar{\mathbf{x}}_0^* - \bar{\mathbf{x}}_H^*\|_{\mathbf{Q}}^2 \leq d \|\bar{\mathbf{x}}_H - \mathbf{x}_g\|_{\mathbf{Q}_e}^2.$$

This result applies given the convex steady-state manifold, the strictly convex quadratic cost, the fact that steady-states are

the interior of the (tightened) constraints with $\epsilon > 0$, and controllability of (\mathbf{A}, \mathbf{B}) with $H \geq 2$. \square

Notably, Theorem 1 relies only on convex optimization, provides robustness guarantees for uncertain nonlinear manipulators, accounts for velocity/acceleration dependence of the model error, and provides a larger region of attraction.¹

VI. CONVEX OBSTACLE AVOIDANCE

In the following section, we adapt the MPC such that we obtain obstacle avoidance guarantees and propose an algorithm that computes the intermediate goals for the MPC, such that the robot is guided through the non-convex collision-free region to reach a given goal state. First, we focus on how to enforce collision avoidance for the MPC in Section VI-A. Our approach uses a SCDF to produce collision-free regions in the form of balls. Obstacle avoidance reduces to requiring that each state in the predicted trajectory should stay inside a corresponding ball, which keeps the convexity of the MPC, resulting in a problem we can solve efficiently. Next, we focus on the maneuvering in Section VI-B. We first sweep the SCDF around a collision-free path, which produces a collision-free region, which we refer to as a corridor. Then we enforce the predicted trajectory of the MPC to stay inside the corridor while making progress towards the goal state through a computed proxy goal.

A. Obstacle avoidance through SCDF

The SCDF is defined as

$$\mathbf{r}(\mathbf{q}) = \begin{cases} -\min_{\mathbf{q}_c \in \partial \mathcal{C}_o} \|\mathbf{q} - \mathbf{q}_c\| & \text{if } \mathbf{q} \in \mathcal{C}_o, \\ \min_{\mathbf{q}_c \in \partial \mathcal{C}_o} \|\mathbf{q} - \mathbf{q}_c\| & \text{otherwise,} \end{cases} \quad (19)$$

which is the distance to the boundary of the obstacle region $\partial \mathcal{C}_o$. Given a collision-free point $\mathbf{c} \in \mathcal{C}_f$, the SCDF allows us to define a collision-free region as

$$\mathcal{B}(\mathbf{c}) = \{\mathbf{q} \in \mathbb{R}^{n_c} \mid \|\mathbf{q} - \mathbf{c}\| \leq \mathbf{r}(\mathbf{c})\} \subseteq \mathcal{C}_f, \quad (20)$$

which is parametrized by the tuple (\mathbf{c}, r) . The region is an Euclidean norm ball in the configuration space. Obtaining an analytical expression for the SCDF is non-trivial, which is why we resort to approximating it using deep learning [11], resulting in a function that can be evaluated efficiently. To adapt the proposed MPC such that it guarantees obstacle avoidance, we simply add the following constraints

$$\begin{aligned} \mathbf{q}(\bar{\mathbf{x}}_i) &\in \mathcal{B}_i \ominus \mathcal{E}_q(\delta_i), \quad i \in \mathbb{N}_{0:H-1}, \\ \mathbf{q}(\bar{\mathbf{x}}_H) &\in \mathcal{B}_H \ominus \mathcal{E}_q(\delta_H + \epsilon), \end{aligned} \quad (21)$$

to the MPC (18). The computation of the constraint tightening is given in Appendix D. In the above, each state in the predicted nominal trajectory is constrained to lie within an allocated ball \mathcal{B}_i . How these are computed is the topic of the next section.

¹Suppose $c = 0$, i.e., the uncertainty in gravity (9) is negligible. Then, any steady-state $\mathbf{x}(0) \in \mathcal{X} \ominus \mathcal{E}(\epsilon)$ is a feasible initial condition of the MPC (18).

Algorithm 1 Our corridor planning approach to control the manipulator to a goal state while avoiding obstacles.

```

1: learn SCDF                                     ▷ Offline part
2:  $a, b, c \leftarrow$  estimate constants (7)-(9)
3:  $\mathcal{A} \leftarrow$  convexify acceleration constraints (17)
4:  $\mathbf{P}, \mathbf{K} \leftarrow$  solve optimization problem, see Appendix B
5:  $\mathbf{x}_g \leftarrow$  get desired goal                  ▷ Online part
6:  $k \leftarrow 0, \mathbf{x}(0) \leftarrow$  measure state
7:  $\gamma \leftarrow$  run path planner
8:  $C, B \leftarrow$  discretize  $\gamma$  and compute SCDF
9:  $\bar{\mathbf{X}} \leftarrow [\mathbf{x}(0)]_{i=0}^H$ 
10: while  $\|\mathbf{x}(k) - \mathbf{x}_g\| > \varepsilon$  do
11:    $\bar{\mathbf{B}} \leftarrow$  assign balls with  $\bar{\mathbf{X}}$  (22)
12:    $\tilde{\mathbf{x}}_g \leftarrow$  select virtual goal (23) with  $C$  and  $\mathcal{B}_H$ 
13:    $\bar{\mathbf{X}}, \bar{\mathbf{A}} \leftarrow$  solve MPC, (18) and (21), with  $\mathbf{x}(k), \tilde{\mathbf{x}}_g, \bar{\mathbf{B}}$ 
14:   for  $i \in \mathbb{N}_{0:n_a-1}$  do
15:      $\bar{\mathbf{a}}, \bar{\mathbf{x}} \leftarrow$  get  $i$ -th reference state and control
16:     apply  $\mathbf{u} = \pi_{FL}(\mathbf{q}, \dot{\mathbf{q}}, \mathbf{a})$  with  $\mathbf{a}$  according to (10)
17:      $\mathbf{x}(k+1) \leftarrow$  measure next state
18:      $k \leftarrow k + 1$ 
19:   end for
20:    $\bar{\mathbf{X}} \leftarrow$  shift  $n_a$  times and append  $[\bar{\mathbf{x}}_H]_{i=1}^{n_a}$ 
21: end while

```

B. Robust corridor planning

Having obtained collision avoidance constraints, we now propose an algorithm that ensures that the robot reaches a given goal configuration, \mathbf{q}_g , without collisions. The high-level idea is to first generate a collision-free region that connects the current configuration and the goal configuration. We refer to this region as a corridor, which is produced using the SCDF around a collision-free path and is illustrated in the left part of Figure 2. Then, we constrain the predicted MPC trajectory to stay within this corridor and pull it towards a temporary virtual goal state, $\tilde{\mathbf{x}}_g$, such that we make progress to the global goal state.

Our approach is sketched in Algorithm 1. Before any planning can take place, we perform the offline tasks already described in the previous sections. That is, we compute the model error constants, line 2, convexify the acceleration constraints, line 3, and compute the auxiliary controller, line 4. Having accomplished the offline part, we are ready to enter the online part. First we receive a collision-free goal state, line 6. Then, we plan a high-level collision-free path, $\gamma(s) : [0, 1] \mapsto \mathcal{C}_f$, to the goal, e.g. by using a sampling-based planner, line 8. Next, in line 9, we discretize the corresponding path with a constant step size, resulting in the sequence $C = (\mathbf{c}_1, \dots, \mathbf{c}_M) \in \mathcal{C}_f^M$, and precompute the collision-free balls with the SCDF according to (20), resulting in a discretized corridor $B = ((\mathbf{c}_1, r_1), \dots, (\mathbf{c}_M, r_M))$.

Having produced a corridor, we now enter the real-time control part, which we initialize with a collision-free feasible trajectory $\bar{\mathbf{X}}$ that stays at the initial steady-state $\mathbf{x}(0)$, line 10.

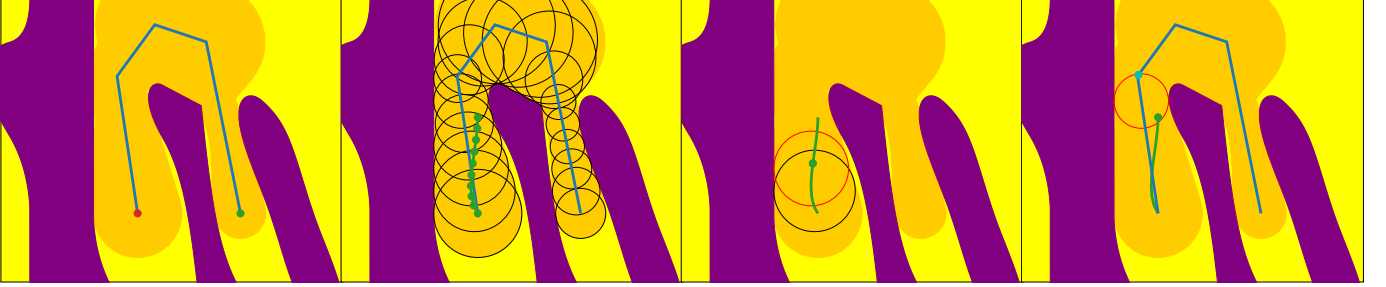


Fig. 2: All plots are illustrated in the configuration space. The yellow and purple symbolize the free and the obstacle regions, respectively. **Left:** From a collision-free path (blue line) a corridor is defined by the SCDF (orange region) **Mid left:** The corridor is discretized, resulting in a sequence of balls (black circles). The idea is to select a set of collision-free balls and a temporary goal state, such that the predicted trajectory makes progress to the goal and stays within the corridor. A feasible trajectory, e.g. trajectory from previous iteration, is used as help (dotted green curve). **Mid right:** The first step is to compute the balls. For each state along a given feasible trajectory, a ball is allocated. An example state is highlighted (green point). The balls that contain the state are selected (black and red circles) then the ball which has the largest margin to the point is selected (red circle). **Right:** Illustration of how the virtual goal is computed. The ball corresponding to the last point along the trajectory is selected (red circle). Then, a virtual goal (cyan point) is computed by finding a point along the path, contained inside the ball, with the furthest progress along the path.

Then we enter the loop, illustrated at an arbitrary iteration in the mid-left part of Figure 2. From a feasible trajectory we loop over all its states $\bar{\mathbf{x}}_i \in \bar{\mathbf{X}}$ and assign a corresponding ball to it, line 12. This is done according to

$$(\mathbf{c}_i, r_i) = \arg \max_{(\mathbf{c}_j, r_j) \in \mathcal{B}} \{r_j - \|\mathbf{q}(\bar{\mathbf{x}}_i) - \mathbf{c}_j\|\}, \quad (22)$$

which returns the ball $\mathcal{B}_i = \mathcal{B}(\mathbf{c}_i)$ that contains $\mathbf{q}(\bar{\mathbf{x}}_i)$ with the largest margin. The assignment rule is conceptualized in the mid right part of Figure 2. The process is repeated for $i \in \mathbb{N}_{0:H}$, resulting in the sequence $\bar{\mathcal{B}} = (\mathcal{B}_0, \dots, \mathcal{B}_H)$.

Next, we compute a virtual goal state, line 13, which serves the purpose of pulling the trajectory in a direction that makes progress to the global goal state. This is done by selecting the configuration that has made the most progress along the path and is contained in the last ball, i.e. according to

$$\tilde{\mathbf{c}}_g = \arg \max_{\mathbf{c}_i \in \mathcal{C}} \{i \mid \mathbf{c}_i \in \mathcal{B}_H \ominus \mathcal{E}_{\mathbf{q}}(\epsilon + \delta_f)\}, \quad (23)$$

where the last ball is tightened with the steady state tube size in order to be compliant with the convergence properties of Theorem 1. Having computed a virtual goal configuration, we define the resulting state as $\tilde{\mathbf{x}}_g = (\tilde{\mathbf{c}}_g, \mathbf{0}_{n_e})$. We illustrate this process in the right part of Figure 2. We continue with solving our adapted MPC problem, line 14, where we solve the MPC problem in (18) using the additional collision avoidance constraints (21) with balls $\bar{\mathcal{B}}$ and the virtual goal $\tilde{\mathbf{x}}_g$ as inputs. Solving the problem results in an optimized nominal trajectory and control inputs. We then enter an inner loop, where we run our auxiliary controller for $n_a \in \mathbb{N}_{1:H}$ steps, line 15 to 20. The number of auxiliary steps is defined by the user, which can help meet the real-time criteria in case solving the MPC takes too long time. Finally, we shift our nominal trajectory n_a times and append the last state n_a times. This is done in order to have a feasible trajectory for the next iteration. The process is repeated until we enter an

ϵ -ball around the global goal state, line 11.

Convergence analysis: The intermediate goal $\tilde{\mathbf{c}}_g$ can only progress up to M times, given the M discretization points. For a constant intermediate goal $\tilde{\mathbf{c}}_g$, Theorem 1 ensures a decrease of the optimal cost and convergence to the goal $\tilde{\mathbf{c}}_g$. If we are close to an intermediate goal $\tilde{\mathbf{c}}_g$, \mathcal{B}_H is centered around it and thus $\tilde{\mathbf{c}}_g$ can advance if the distance to obstacles (modulo the tightening) is larger than the distance to the next intermediate goal. This is ensured through a fine enough discretization. Overall, by adding the ball constraints (21) and an intermediate goal $\tilde{\mathbf{c}}_g$, both computed with the corridor planner, to the MPC (18), the proposed approach successfully navigates non-convex obstacles and reaches the goal.

VII. NUMERICAL EXPERIMENTS

A. Setup

1) Robot: The robot we use for our simulations is an IRB 1100 which is a six DOF robot, illustrated in the left part of Figure 3. The robots nominal acceleration constraint is defined as $\mathcal{A} = \{\mathbf{a} \in \mathbb{R}^{n_c} \mid \|\mathbf{a}\|_{\infty} \leq 20\}$. The configuration space and the velocity constraint set is defined as $\mathcal{C} = \{\mathbf{q} \in \mathbb{R}^{n_c} \mid \|\mathbf{q}\|_{\infty} \leq \pi\}$ and $\mathcal{V} = \{\dot{\mathbf{q}} \in \mathbb{R}^{n_c} \mid \|\dot{\mathbf{q}}\|_{\infty} \leq 2\}$, respectively. For our coupling matrix, we use both damping and the Coriolis matrix. Our damping matrix is defined as $\text{diag}([10^{-1}, 10^{-1}, 10^{-1}, 10^{-2}, 10^{-2}, 10^{-4}]) \cdot 2$. The other dynamics, e.g. Coriolis, are computed from calibrated model data of an IRB 1100. To understand how the problem scales with increasing number of DOFs, we divide the problem into a 3 and 6 DOF case. For the 3 DOF case, we focus on the first three joints, while in the other scenario we include all joints. We consider parametric uncertainty in the mass of each link and the damping matrix. We define 5% and 0.75% uncertainty as the nominal values for the 3 DOF and 6 DOF cases, respectively. To study the effect of different values of uncertainty, we scale the nominal values according to

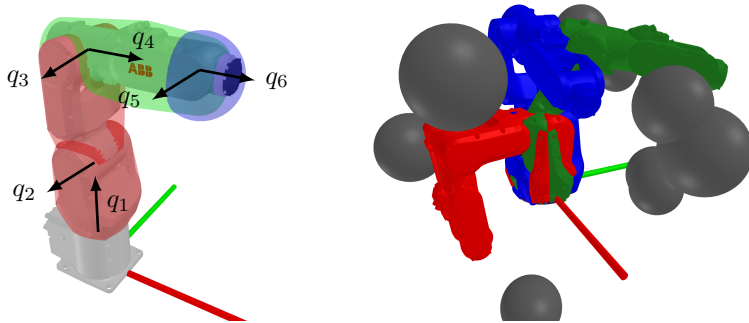


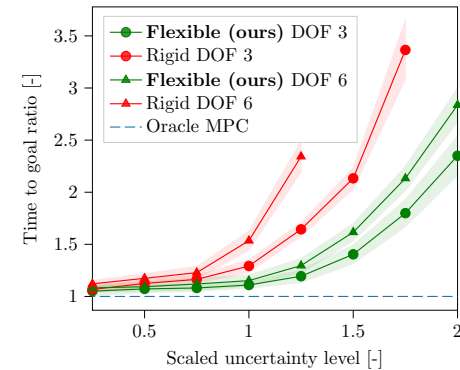
Fig. 3: **Left:** Robot collision-geometry. The wrist axes are over approximated with a sphere (blue mesh). **Middle:** Illustrates the problem setup and a solved problem instance. The obstacles are represented by the gray spheres. The robot's configurations at the start, goal, and an intermediate point along the solved trajectory are depicted in red, green, and blue, respectively. **Right:** The horizontal axis presents scaled uncertainties, where 1 corresponds to 5% and 0.75% for the 3 and 6 DOF case, respectively. The vertical axis presents the time duration to goal divided with the time it takes for an Oracle MPC, which is a nominal MPC without any model errors. Thus, values closer to one are better. Rigid refers to a fixed sized tube, Flexible refers to our approach. A nominal MPC methods was also tested, but it failed to reach the goal region in all problem instances due to infeasibility. No method was able to safely reach the goal for a scaled uncertainty larger than 2.5.

$\{0.25, 0.5, 0.75, 1.0, 1.25, 1.5, 1.75, 2.0\}$. We assume perfect estimation of gravity, i.e. $c = 0$ in (9).

2) *Obstacle avoidance:* The SCDF is approximated by using the learning approach presented in [11]. The approach is currently limited to 3 DOF, but we addressed this by over-approximating the wrist axes, i.e. the last axes of the robot, with a sphere, effectively reducing the obstacle avoidance problem to 3 DOF. The collision geometries are presented in the left part of Figure 3. A world space instance is constructed by sampling 10 random spheres, with different sizes and positions, illustrated in the middle part of Figure 3. The obstacles were not seen when learning the SCDF and the SCDF was not re-learned at this stage. We sample in total 10 world instances, for each instance we sample a start and goal configuration, ignoring pairs which can be connected with a collision-free straight line. We find a collision-free path using RRT-Connect [26]. To gain overall clearance in the paths, we use the SCDF in the path planner and require a clearance of 0.1 [rad]. Next, we discretize the path equidistantly with a step size of 0.001 [rad] and 0.005 [rad] for the 3 and 6 DOF cases, respectively. Then we query the SCDF for the distances of all the points.

3) *Benchmarks:* In addition to our method, we run a nominal MPC and a rigid tube MPC, which serves as benchmarking methods. The same approach to corridor planning is used. The nominal MPC is the same MPC as in (18), but without the robustness features, i.e., $\delta = 0$. The rigid tube MPC is executed with a constant constraint tightening δ_i . All methods are executed with the the following parameters: $H = 20$, $\mathbf{Q} = \text{diag}([\mathbf{1}_{n_c}^\top \cdot 10, \mathbf{1}_{n_c}^\top \cdot 0.01]^\top)$, $\mathbf{Q}_e = \text{diag}(\mathbf{1}_{n_x} \cdot 10^4)$ and $\mathbf{R} = \text{diag}(\mathbf{1}_{n_c} \cdot 10^{-3})$. The robust MPC problems are solved using Clarabel [27], which is done every $n_a = 4$ steps to ensure real-time feasibility.

4) *Simulations:* All simulations are done in discrete-time, i.e. through (5), with a time step of 10 ms. For each run, we sample the uncertain parameters $\theta \in \Theta$ uniformly. If the



method was not able to reach the goal within 4000 steps (40 seconds), it was stopped and labeled as unsuccessful. To verify the SCDF, we collision-checked all trajectories returned from the methods with a conventional collision checker [28] using the exact obstacle and robot geometries. The robot was defined to have reached the goal if its state is within an ε -ball of radius 0.01 around the goal state. We measure performance based on the time it takes to reach the goal region and how it scales with increasing uncertainty.

B. Results

The results from the experiments are presented in the right part of Figure 3. The horizontal axis presents a scaled uncertainty level, where 1.0 represents 5% and 0.75% uncertainty for the 3 DOF and 6 DOF case, respectively. The curves presents the average time ratio over all successful problem instances, while the shaded region around the curves covers 2 standard deviations. None of the methods resulted in trajectories that were in collision. The nominal MPC is not included in the figure since it resulted in infeasibility issues in each run due to the model errors. This shows the importance of including robustness in the design. For the robust methods, larger uncertainty yields a longer time to reach the goal due to the larger tube. While the variance increases with increased uncertainty, it's relatively small, highlighting that the robust approach is insensitive to the specific model parameters $\theta \in \Theta$ and to the start/goal configuration. Comparing the performance between the robust methods, we see that rigid tube MPC is significantly slower and fails to scale to larger uncertainties, since the tightening is too conservative. Thus, having a flexible tube lowers the conservativeness, making our approach applicable to larger uncertainties, while also yielding faster motions compared to the fixed tube approach.

The offline computation times are presented in Table I, showing larger computation times for increasing DOFs.

TABLE I: Average computation times for the offline tasks.

Offline task	Avg. computation time [s]	
	DOF 3	DOF 6
SCDF	32000	
Convex acceleration set (17)	1	4
Model error constants (7)-(9)	1700	7900
Computing controller (Appendix B)	30	4600

Regarding the online computation times, finding a path takes on average 30 [ms], which is only executed when a new goal q_g is set. For the real-time control, assigning the balls and computing the virtual goal takes on average 2 [ms] and 3 [ms] for the 3 and 6 DOF cases, respectively. The difference is due to the smaller discretization used for the 3 DOF case. The main computational bottleneck is the computation time of solving the MPC problem, which we present in Table II.

TABLE II: Average computation times for MPC problems.

MPC method	Avg. MPC solve time [ms]	
	DOF 3	DOF 6
Nominal	6	11
Rigid tube	9	20
Flexible tube (ours)	13	30

We see that without robustness features, computation times are lower. Adding robustness properties more or less doubles the computation time, where our approach is the most computationally heavy one. However, since we take $n_a = 4$ time steps with our auxiliary controller in the inner loop, we are real-time feasible (time step of 10 [ms]).

In summary, our MPC resulted in the fastest motion, remained safe at all times, while also scaling to higher uncertainties.

VIII. CONCLUSIONS

We have presented a novel convex robust motion planning solution for manipulators that gives robustness guarantees to bounded model errors and results in collision-free motion. One of the main benefits is that we derived a convex optimization problem, which can be solved fast and reliably. From the numerical experiments, we observed that a robust design of the MPC is necessary to maintain feasibility. Compared to a more standard robust MPC formulation, our approach was less conservative, resulting in faster motion, and scaled to larger levels of uncertainty.

REFERENCES

- [1] S. M. LaValle, *Planning algorithms*. Cambridge university press, 2006.
- [2] S. LaValle, “Rapidly-exploring random trees: A new tool for path planning,” *Research Report 9811*, 1998.
- [3] L. Kavraki, P. Svestka, J.-C. Latombe, and M. Overmars, “Probabilistic roadmaps for path planning in high-dimensional configuration spaces,” *IEEE Transactions on Robotics and Automation*, vol. 12, no. 4, pp. 566–580, 1996.
- [4] K. Hauser and V. Ng-Thow-Hing, “Fast smoothing of manipulator trajectories using optimal bounded-acceleration shortcuts,” in *International Conference on Robotics and Automation (ICRA)*, 2010.
- [5] D. Verschueren, B. Demeulenaere, J. Swevers, J. De Schutter, and M. Diehl, “Time-optimal path tracking for robots: A convex optimization approach,” *IEEE Transactions on Automatic Control*, vol. 54, no. 10, pp. 2318–2327, 2009.
- [6] B. Siciliano, L. Sciavicco, L. Villani, and G. Oriolo, *Robotics: Modelling, Planning and Control*. Springer Publishing Company, 2008.
- [7] K. Lynch and F. Park, *Modern Robotics: Mechanics, Planning, and Control*. Cambridge University Press, 2017.
- [8] A. Amice, H. Dai, P. Werner, A. Zhang, and R. Tedrake, “Finding and optimizing certified, collision-free regions in configuration space for robot manipulators,” in *International Workshop on the Algorithmic Foundations of Robotics*, pp. 328–348, Springer, 2022.
- [9] M. Petersen and R. Tedrake, “Growing convex collision-free regions in configuration space using nonlinear programming,” *arXiv preprint arXiv:2303.14737*, 2023.
- [10] Y. Li, X. Chi, A. Razmjoo, and S. Calinon, “Configuration space distance fields for manipulation planning,” *arXiv preprint arXiv:2406.01137*, 2024.
- [11] B. Wullt, M. Norrlöf, P. Mattsson, and Thomas B. Schön, “Probabilistic Bubble Roadmap.” <https://arxiv.org/abs/2502.16205>, 2025.
- [12] R. Geraerts and M. H. Overmars, “The corridor map method: Real-time high-quality path planning,” in *IEEE International Conference on Robotics and Automation (ICRA)*, IEEE, 2007.
- [13] F. Gao, W. Wu, W. Gao, and S. Shen, “Flying on point clouds: Online trajectory generation and autonomous navigation for quadrotors in cluttered environments,” *Journal of Field Robotics*, vol. 36, no. 4, pp. 710–733, 2019.
- [14] Y. Ren, F. Zhu, W. Liu, Z. Wang, Y. Lin, F. Gao, and F. Zhang, “Bubble planner: Planning high-speed smooth quadrotor trajectories using receding corridors,” in *2022 IEEE/RSJ International Conference on Intelligent Robots and Systems (IROS)*, pp. 6332–6339, IEEE, 2022.
- [15] C. K. Verginis, D. V. Dimarogonas, and L. E. Kavraki, “KDF: Kinodynamic motion planning via geometric sampling-based algorithms and funnel control,” *IEEE Transactions on Robotics*, vol. 39, no. 2, pp. 978–997, 2023.
- [16] F. Borrelli, A. Bemporad, and M. Morari, *Predictive control for linear and hybrid systems*. Cambridge University Press, 2017.
- [17] J. Nubert, J. Köhler, V. Berenz, F. Allgöwer, and S. Trimpe, “Safe and fast tracking on a robot manipulator: Robust MPC and neural network control,” *IEEE Robotics and Automation Letters*, vol. 5, no. 2, pp. 3050–3057, 2020.
- [18] A. Carron, E. Arcari, M. Wermelinger, L. Hewing, M. Hutter, and M. N. Zeilinger, “Data-driven model predictive control for trajectory tracking with a robotic arm,” *IEEE Robotics and Automation Letters*, vol. 4, no. 4, pp. 3758–3765, 2019.
- [19] G. P. Incremona, A. Ferrara, and L. Magni, “MPC for robot manipulators with integral sliding modes generation,” *IEEE/ASME Transactions on Mechatronics*, vol. 22, no. 3, pp. 1299–1307, 2017.
- [20] P. M. Julbe, J. Nubert, H. Hose, S. Trimpe, and K. J. Kuchenbecker, “Diffusion-based approximate MPC: Fast and consistent imitation of multi-modal action distributions,” *arXiv preprint arXiv:2504.04603*, 2025.
- [21] L. Li, Y. Miao, A. H. Qureshi, and M. C. Yip, “MPC-MPNet: Model-predictive motion planning networks for fast, near-optimal planning under kinodynamic constraints,” *IEEE Robotics and Automation Letters*, vol. 6, no. 3, pp. 4496–4503, 2021.
- [22] R. A. Horn and C. R. Johnson, *Matrix analysis*. Cambridge university press, 2012.
- [23] P. Krupa, J. Köhler, A. Ferramosca, I. Alvarado, M. N. Zeilinger, T. Alamo, and D. Limon, “Model predictive control for tracking using artificial references: Fundamentals, recent results and practical implementation,” in *Proc. Conf. Decision and Control (CDC)*, 2024.
- [24] A. Sasfi, M. N. Zeilinger, and J. Köhler, “Robust adaptive MPC using control contraction metrics,” *Automatica*, vol. 155, p. 111169, 2023.
- [25] J. Köhler, M. A. Müller, and F. Allgöwer, “Analysis and design of model predictive control frameworks for dynamic operation—an overview,” *Annual Reviews in Control*, vol. 57, p. 100929, 2024.
- [26] J. J. Kuffner and S. M. LaValle, “RRT-Connect: An efficient approach to single-query path planning,” in *IEEE International Conference on Robotics and Automation (ICRA)*, 2000.
- [27] P. J. Goulart and Y. Chen, “Clarabel: An interior-point solver for conic programs with quadratic objectives,” *arXiv preprint arXiv:2405.12762*, 2024.
- [28] Dawson-Haggerty, “trimesh,” 2019.
- [29] S. Boyd, L. El Ghaoui, E. Feron, and V. Balakrishnan, *Linear matrix inequalities in system and control theory*. SIAM, 1994.

APPENDIX

A. Model error derivation

In the following, to increase readability, we drop the input arguments to the functions, e.g. $\mathbf{M} = \mathbf{M}(\mathbf{q})$. From the manipulator dynamics (1) we obtain

$$\begin{aligned}\ddot{\mathbf{q}} &= \mathbf{M}^{-1}(\mathbf{u} - \mathbf{C}\dot{\mathbf{q}} - \mathbf{g}) \\ &\stackrel{\text{FL}}{=} \mathbf{M}^{-1}(\mathbf{M}_0\mathbf{a} + \mathbf{C}_0\dot{\mathbf{q}} + \mathbf{g}_0 - (\mathbf{C}_0 + \mathbf{C}_\theta)\dot{\mathbf{q}} - (\mathbf{g}_0 + \mathbf{g}_\theta)) \\ &= \mathbf{M}^{-1}\mathbf{M}_0\mathbf{a} - \mathbf{M}^{-1}\mathbf{C}_\theta\dot{\mathbf{q}} - \mathbf{M}^{-1}\mathbf{g}_\theta \\ &\stackrel{*}{=} (\mathbf{I} + \tilde{\mathbf{M}}_\theta)\mathbf{a} - \mathbf{M}^{-1}\mathbf{C}_\theta\dot{\mathbf{q}} - \mathbf{M}^{-1}\mathbf{g}_\theta \\ &= \mathbf{a} + \tilde{\mathbf{M}}_\theta\mathbf{a} - \mathbf{M}^{-1}\mathbf{C}_\theta\dot{\mathbf{q}} - \mathbf{M}^{-1}\mathbf{g}_\theta \\ &= \mathbf{a} + \Delta_\theta(\mathbf{q}, \dot{\mathbf{q}}, \mathbf{a}).\end{aligned}$$

In the above, FL denotes feedback linearization. The $*$ denotes the step where we decompose the matrix in front of the acceleration input into $\mathbf{I} + \tilde{\mathbf{M}}_\theta$ as follows

$$\begin{aligned}(\mathbf{M}_0 + \mathbf{M}_\theta)^{-1}\mathbf{M}_0 &= \mathbf{I} + \tilde{\mathbf{M}}_\theta \\ \mathbf{M}_0 &= (\mathbf{M}_0 + \mathbf{M}_\theta) + (\mathbf{M}_0 + \mathbf{M}_\theta)\tilde{\mathbf{M}}_\theta \\ \tilde{\mathbf{M}}_\theta &= -(\mathbf{M}_0 + \mathbf{M}_\theta)^{-1}\mathbf{M}_\theta\end{aligned}\quad (24)$$

The function $\Delta_\theta(\mathbf{q}, \dot{\mathbf{q}}, \mathbf{a}) : \mathbb{R}^{n_x} \times \mathbb{R}^{n_u} \mapsto \mathbb{R}^{n_c}$ defines the state and input dependent model error on the following form

$$\Delta(\mathbf{q}, \dot{\mathbf{q}}, \mathbf{a}) = \tilde{\mathbf{M}}_\theta\mathbf{a} + \tilde{\mathbf{C}}_\theta\dot{\mathbf{q}} + \tilde{\mathbf{g}}_\theta, \quad (25)$$

$$\tilde{\mathbf{M}}_\theta = -\mathbf{M}^{-1}\mathbf{M}_\theta, \quad (26)$$

$$\tilde{\mathbf{C}}_\theta = -\mathbf{M}^{-1}\mathbf{C}_\theta, \quad (27)$$

$$\tilde{\mathbf{g}}_\theta = -\mathbf{M}^{-1}\mathbf{g}_\theta. \quad (28)$$

B. Auxiliary controller and Lyapunov matrix

We present the optimization problem to compute \mathbf{P}, \mathbf{K} in Appendix B1, and derive it in Appendix B2. How we selected a suitable pair \mathbf{P} and \mathbf{K} in the experiments is presented in Appendix B3.

1) *Convex optimization program:* We solve the following semidefinite program to produce the gain \mathbf{K} and Lyapunov matrix \mathbf{P} :

$$\min_{\mathbf{E}, \mathbf{Y}, c_{x,i}^2, c_{u,j}^2, \bar{w}^2} L(\bar{w}^2, c_{x,1}^2, \dots, c_{x,m}^2, c_{u,1}^2, \dots, c_{u,n}^2) \quad (29a)$$

$$\text{s.t. } \begin{bmatrix} \rho^2\mathbf{E}, (\mathbf{A}\mathbf{E} + \mathbf{B}\mathbf{Y})^\top \\ (\mathbf{A}\mathbf{E} + \mathbf{B}\mathbf{Y})^\top, \mathbf{E} \end{bmatrix} \succcurlyeq 0 \quad (29b)$$

$$\begin{bmatrix} c_{x,i}^2, [\mathbf{A}_x]_i \mathbf{E} \\ ([\mathbf{A}_x]_i \mathbf{E})^\top, \mathbf{E} \end{bmatrix} \succcurlyeq 0, \forall i \in \mathbb{N}_{1:m}, \quad (29c)$$

$$\begin{bmatrix} c_{u,i}^2, [\mathbf{A}_u]_i \mathbf{Y} \\ ([\mathbf{A}_u]_i \mathbf{Y})^\top, \mathbf{E} \end{bmatrix} \succcurlyeq 0, \forall j \in \mathbb{N}_{1:n}, \quad (29d)$$

$$\begin{bmatrix} \bar{w}^2, \mathbf{v}_\mathcal{W}^\top \\ \mathbf{v}_\mathcal{W}, \mathbf{E} \end{bmatrix} \succcurlyeq 0, \forall \mathbf{v}_\mathcal{W} \in \text{vertex}(\mathcal{W}), \quad (29e)$$

with the objective function defined as

$$\begin{aligned}L(\bar{w}^2, c_{x,1}^2, \dots, c_{x,m}^2, c_{u,1}^2, \dots, c_{u,n}^2) &= \\ \frac{1}{2(1-\rho)} \left((m+n)\bar{w}^2 + \sum_{i=1}^m c_{x,i}^2 + \sum_{i=1}^n c_{u,i}^2 \right). \quad (30)\end{aligned}$$

The gain and Lyapunov matrix is computed from the following relationship $\mathbf{E} = \mathbf{P}^{-1}$ and $\mathbf{Y} = \mathbf{K}\mathbf{E}$. The decision variables $c_{x,i}^2, i \in \mathbb{N}_{1:m}$ and $c_{u,j}^2, j \in \mathbb{N}_{1:n}$, control the amount of tightening on the state and control constraints, respectively. In this context, the set \mathcal{W} is a box set of the model error and vertex(\cdot), outputs its vertex representation. The inputs are the state constraints, $\mathbf{A}_x \in \mathbb{R}^{m \times n_x}$ and $\mathbf{b}_x \in \mathbb{R}^m$, the control input constraints, $\mathbf{A}_u \in \mathbb{R}^{n \times n_u}$ and $\mathbf{b}_u \in \mathbb{R}^n$, and the contraction rate, $\rho \in (0, 1)$. We assume polytopic constraints, represented in its half-plane form, i.e. for the state constraints the form is

$$\mathcal{X} = \{\mathbf{x} \in \mathbb{R}^{n_x} \mid [\mathbf{A}_x]_i \mathbf{x} \leq b_{x,i}, i \in \mathbb{N}_{1:m}\}, \quad (31)$$

where $[\mathbf{A}_x]_i$ is the i :th row of the matrix \mathbf{A}_x and $b_{x,i}$ is the i :th element of \mathbf{b}_x .

2) *Derivation of optimization problem:* Our goal is to derive an optimization problem where the amount of tightening is included in the cost, thereby allowing us to reduce the conservatism in the tightening.

In order to achieve this, we first have to derive an expression for the tightened state and input constraints. Then, we present LMI's which allows us to include the tightening in the optimization. This results in a non-convex objective which we as a last step convexify, ending up with our proposed optimization problem.

First, the following linear matrix inequalities (LMIs) are a standard reformulation of inequality (11) (cf. [29]):

$$\begin{bmatrix} \rho^2\mathbf{E}, (\mathbf{A}\mathbf{E} + \mathbf{B}\mathbf{Y})^\top \\ (\mathbf{A}\mathbf{E} + \mathbf{B}\mathbf{Y})^\top, \mathbf{E} \end{bmatrix} \succcurlyeq 0. \quad (32a)$$

The worst case disturbance is defined as

$$\bar{w} = \max_{\mathbf{w} \in \mathcal{W}} \|\mathbf{w}\|_{\mathbf{P}}, \quad (33)$$

A robust positive invariant (RPI) set can be computed that contains the worst case disturbance, having the following tube size

$$\bar{\delta} = \frac{\bar{w}}{1-\rho}. \quad (34)$$

The rigid tube MPC in Section VII-A3 uses the above tube size to tighten its constraints.

Next, we focus on how to introduce the tightenings into the optimization problem. We start by deriving an expression for the state constraint tightening. We require that around a reference state, $\bar{\mathbf{x}}$, the tube with size δ should not violate the state constraints. That is, for each $i \in \mathbb{N}_{1:m}$, we want

$$[\mathbf{A}_x]_i \mathbf{x} \leq b_{x,i}, \forall \mathbf{x} : \|\mathbf{x} - \bar{\mathbf{x}}\|_{\mathbf{P}} \leq \delta. \quad (35)$$

The error is defined as $\mathbf{e} = \mathbf{x} - \bar{\mathbf{x}}$. We introduce

$$\mathbf{e} = \mathbf{P}^{-1/2}\tilde{\mathbf{e}}. \quad (36)$$

Now, we input the above into the condition of (35) resulting in

$$[\mathbf{A}_x]_i(\bar{\mathbf{x}} + \mathbf{P}^{-1/2}\tilde{\mathbf{e}}) \leq b_{x,i}, \forall \|\tilde{\mathbf{e}}\| \leq \delta. \quad (37)$$

The worst case error maximizer is the following

$$\tilde{\mathbf{e}}^* = \frac{([\mathbf{A}_x]_i \mathbf{P}^{-1/2})^\top}{\|([\mathbf{A}_x]_i \mathbf{P}^{-1/2})^\top\|} \delta. \quad (38)$$

Thus, the tightened constraints become

$$[\mathbf{A}_x]_i \bar{\mathbf{x}} + \|([\mathbf{A}_x]_i \mathbf{P}^{-1/2})^\top\| \delta \leq b_{x,i}, \quad (39)$$

and we define the tightening constants as

$$c_{x,i} = \|([\mathbf{A}_x]_i \mathbf{P}^{-1/2})^\top\|. \quad (40)$$

Next, we focus on the control input tightening. Using the control law in (10), $\mathbf{a} = \bar{\mathbf{a}} + \mathbf{K}(\mathbf{x} - \bar{\mathbf{x}})$, into the above we get

$$[\mathbf{A}_u]_j \bar{\mathbf{a}} + [\mathbf{A}_u]_j \mathbf{K} \mathbf{e} \leq b_{u,j}. \quad (41)$$

This is on the same form as for the state constraints. Thus, following the same approach, the tightening constant can be expressed as

$$c_{u,j} = \|([\mathbf{A}_u]_j \mathbf{K} \mathbf{P}^{-1/2})^\top\|. \quad (42)$$

Having introduced the expressions for both the state and control input tightening, we now address how to include them into the optimization problem. We start by re-writing our tightenings. Focusing on the state inputs, for $i \in \mathbb{N}_{1:m}$ then (40) and (34) defines our tightening, which we express as

$$c_{x,i} \bar{\delta} = c_{x,i} \bar{w} \frac{1}{1 - \rho}, \quad (43)$$

and split into two inequalities

$$[\mathbf{A}_x]_i \mathbf{E} [\mathbf{A}_x]_i^\top \leq c_{x,i}^2, \quad (44)$$

$$\max_{\mathbf{w} \in \mathcal{W}} \sqrt{\mathbf{w}^\top \mathbf{P} \mathbf{w}} \leq \bar{w}, \quad (45)$$

where $\mathbf{E} = \mathbf{P}^{-1}$. We rewrite the above into LMI's using the Schur complement [22], ending up with the LMI's in (29c) and (29e). The control input tightenings follows the same reasoning. Now, we include all the state and control input tightenings in the objective, resulting in

$$\frac{1}{1 - \rho} \left(\sum_{i=1}^m c_{x,i} \bar{w} + \sum_{j=1}^n c_{u,j} \bar{w} \right). \quad (46)$$

The bi-linear terms makes the cost non-convex. To make it convex we use the inequality of the arithmetic and geometric means [22], which results in

$$c_{x,i} \bar{w} \leq \frac{1}{2} (c_{x,i}^2 + \bar{w}^2), \quad (47)$$

$$c_{u,j} \bar{w} \leq \frac{1}{2} (c_{u,j}^2 + \bar{w}^2), \quad (48)$$

ending up with the loss in (30).

3) *Candidate selection:* We normalized the objective function by dividing the constraint tightenings of the configuration, velocity and control with a representative normalizing factor. For the configuration tightening, we used 0.1 [rad], which was the padded clearance added in the path planning. For the velocity and control tightening, they were divided with their corresponding max values from the constraints, i.e. 2 [rad/s] and 20 [rad/s²], respectively.

We compute 20 values of ρ , equally spaced between 0.8 and 0.99. Having solved the optimization problem for all values of ρ resulted in 20 pairs of \mathbf{K} and \mathbf{P} . First, all pairs where $\tilde{\rho} \geq 1$ was satisfied were removed. From the remaining pairs, we selected the pair that resulted in the smallest max tightening. For the rigid tube MPC, the condition $\tilde{\rho} \geq 1$ was ignored, otherwise the same selection rule was used.

C. Proof of Proposition 2

It holds that

$$\begin{aligned} \|\mathbf{x}_+ - \bar{\mathbf{x}}_+\|_{\mathbf{P}} &= \|\mathbf{A}_{\text{cl}}(\mathbf{x} - \bar{\mathbf{x}}) + \mathbf{B} \Delta(\mathbf{x}, \mathbf{a})\|_{\mathbf{P}} \\ &\leq \|\mathbf{A}_{\text{cl}}(\mathbf{x} - \bar{\mathbf{x}})\|_{\mathbf{P}} + \|\mathbf{B} \Delta(\mathbf{x}, \mathbf{a})\|_{\mathbf{P}} \\ &\stackrel{(11), \text{ Prop. 1}}{\leq} \rho \|\mathbf{x} - \bar{\mathbf{x}}\|_{\mathbf{P}} + \|\mathbf{P}^{1/2} \mathbf{B}\| \beta(\mathbf{x}, \mathbf{a}), \end{aligned}$$

with $\mathbf{A}_{\text{cl}} = \mathbf{A} + \mathbf{B} \mathbf{K}$. The uncertainty bound β satisfies

$$\begin{aligned} \beta(\mathbf{x}, \mathbf{a}) - \beta(\bar{\mathbf{x}}, \bar{\mathbf{a}}) &\stackrel{(6)}{=} a(\|\mathbf{a}\| - \|\bar{\mathbf{a}}\|) + b(\|\mathbf{V}\mathbf{x}\| - \|\mathbf{V}\bar{\mathbf{x}}\|) \\ &\leq a \|\mathbf{K}(\mathbf{x} - \bar{\mathbf{x}})\| + b \|\mathbf{V}(\mathbf{x} - \bar{\mathbf{x}})\| \\ &\stackrel{(15)}{\leq} L_{\beta} \|\mathbf{x} - \bar{\mathbf{x}}\|_{\mathbf{P}} \leq L_{\beta} \delta. \end{aligned}$$

In the above, $\mathbf{V} = [\mathbf{0}_{n_c \times n_c}, \mathbf{I}]$. Combining both bounds yields

$$\begin{aligned} \|\mathbf{x}_+ - \bar{\mathbf{x}}_+\|_{\mathbf{P}} &\leq \rho \|\mathbf{x} - \bar{\mathbf{x}}\|_{\mathbf{P}} + \|\mathbf{P}^{1/2} \mathbf{B}\| \beta(\mathbf{x}, \mathbf{a}) \\ &\leq \rho \delta + \|\mathbf{P}^{1/2} \mathbf{B}\| (L_{\beta} \delta + \beta(\bar{\mathbf{x}}, \bar{\mathbf{a}})) = \delta_+. \end{aligned}$$

D. Tube in ball constraint

To compute the tightened ball constraints in (21), we compute a ball that over-approximates the projection of the tube on the configuration space:

$$\begin{aligned} \mathcal{E}_{\mathbf{q}}(\delta) &:= \{\mathbf{q}(\mathbf{x}) \in \mathbb{R}^{n_c} \mid \|\mathbf{q}\| \leq \delta \cdot r_p\} \\ &\supseteq \{\mathbf{q}(\mathbf{x}) \in \mathbb{R}^{n_c} \mid \|\mathbf{x} - \bar{\mathbf{x}}\|_{\mathbf{P}} \leq \delta\}, \end{aligned} \quad (49)$$

with a suitable radius $r_p > 0$. To ensure the above, we start by projecting \mathcal{E} onto the configuration space. The Lyapunov matrix is structured as

$$\mathbf{P} = \begin{bmatrix} \mathbf{P}_{11}, \mathbf{P}_{12} \\ \mathbf{P}_{21}, \mathbf{P}_{22} \end{bmatrix}. \quad (50)$$

The projection of the ellipsoid onto the configuration space, $\mathcal{E}_{\mathbf{q}}$, is done with the Schur-complement

$$\mathbf{P}_{\mathbf{q}} = \mathbf{P}_{11} - \mathbf{P}_{12} \mathbf{P}_{22}^{-1} \mathbf{P}_{21}. \quad (51)$$

The eigenvalues give the principal axes of the resulting ellipsoid. We compute a radius that encompasses the projected ellipsoid as

$$r_p = 1 / \sqrt{\lambda_{\min}(\mathbf{P}_{\mathbf{q}})}. \quad (52)$$

Now, to fulfill condition (49), we simply shrink the given ball's radius, r , by $r_p\delta$. Thus our homothetic constraint tightening becomes

$$\mathcal{B} \ominus \mathcal{E}_{\mathbf{q}}(\delta) = \{\mathbf{q} \in \mathbb{R}^{n_c} \mid \|\mathbf{c} - \mathbf{q}\| \leq r - r_p\delta\}. \quad (53)$$